





Simulating the Dark Matter Decay Signal from the Perseus Galaxy Cluster

Mark R. Lovell^{1,2} , Dmytro Iakubovskiy³, David Barnes⁴, Sownak Bose⁵ , Carlos S. Frenk², Tom Theuns², and Wojciech A. Hellwing⁶

¹University of Iceland, Dunhagi 5, 107 Reykjavík, Iceland; lovell@hi.is

²Durham University, South Road, Durham, DH1 3LE, UK

³Bogolyubov Institute of Theoretical Physics, Metrologichna Str. 14-b, 03143, Kyiv, Ukraine

⁴Department of Physics, Kavli Institute for Astrophysics and Space Research, Massachusetts Institute of Technology, Cambridge, MA 02139, USA

⁵Harvard-Smithsonian Center for Astrophysics, 60 Garden Street, Cambridge, MA 02138, USA

⁶Center for Theoretical Physics, Polish Academy of Sciences, Aleja Lotników 32/46, 02-668 Warsaw, Poland

Received 2019 March 14; revised 2019 March 26; accepted 2019 March 26; published 2019 April 19

Abstract

The nearby Perseus galaxy cluster is a key target for indirect detection searches for decaying dark matter. We use the C-EAGLE simulations of galaxy clusters to predict the flux, width, and shape of a dark matter decay line, paying particular attention to the unexplained 3.55 keV line detected in the spectra of some galaxies and clusters, and the upcoming *XRISM* X-ray observatory mission. We show that the line width in C-EAGLE clusters similar to Perseus is typically [600–800] km s^{−1}, and therefore narrower than the amplitude of the velocity dispersion of galaxies in the cluster. Halos that are significantly disturbed can, however, exhibit galaxy velocity dispersions higher than 1000 km s^{−1}, and in this case will show a large difference between the line profiles of on- and off-center observations. We show that the line profile is likely to be slightly asymmetric, but still well approximated by a Gaussian at the 10% level, and that the halo asymmetry can lead to fluxes that vary by a factor of two. In summary, we predict that, if the previously reported 3.55 keV line detections do originate from dark matter decay, the *XRISM* mission will detect a line with a roughly Gaussian profile at a rest-frame energy of 3.55 keV, with a width >600 km s^{−1} and flux approximately in the range [4–9] × 10^{−8} counts s^{−1} cm^{−2}.

Key words: dark matter – galaxies: clusters: general

1. Introduction

One of the possible means for identifying dark matter is the detection of photons that are emitted during the annihilation or decay of dark matter particles in astrophysical objects such as galaxies and clusters of galaxies. The decay channel is favored if the dark matter particle is light ($m_p c^2 \ll \text{GeV}$). An unidentified line feature at an energy of 3.55 keV has been reported in multiple astronomical objects (e.g., Boyarsky et al. 2014, 2018; Bulbul et al. 2014; Cappelluti et al. 2018). One of the possible origins for this line is the decay of a 7.1 keV-mass dark matter particle.

In order to confirm or exclude dark matter decay as the origin for these 3.55 keV photons, multiple targets will have to be observed with X-ray observatories, and their flux amplitudes measured and found to all be consistent with originating from a particle of the same mass and lifetime, as was shown in Lovell et al. (2019). In that paper, one of the most promising targets was the Perseus galaxy cluster, which has the benefit that its predicted line has not two but three properties that can be measured: its flux, its energy, and its line width, the last of which is broad enough to have been resolved by the defunct *Hitomi* mission (Aharonian et al. 2017; Tamura et al. 2018), and will be resolved by the upcoming *XRISM* (~2022; ~5 eV energy resolution) and *ATHENA/XIFU* (~2028; ~2.5 eV energy resolution) missions, as well as the proposed *Lynx/LXM* observatory (>2030; ~3 eV energy resolution). Having a model that describes the height, width, and shape of the Perseus cluster is a crucial component of the search for decaying dark matter. This is complicated, however, by the fact that the dark matter velocity dispersion, and thus the line width, cannot be measured directly from observations, and the most popular proxy for this quantity, the velocity dispersion of the cluster

member galaxies (as considered in Aharonian et al. 2017), may not be sufficiently accurate for our purposes (e.g., Armitage et al. 2018; Elahi et al. 2018).

In this Letter we make predictions for the flux, equivalent width, and shape of the hypothesized dark matter decay line in Perseus using the method based on hydrodynamical cosmological simulations of Lovell et al. (2015, 2019), paying particular attention to the differences between the member galaxy and dark matter velocity dispersions, and also to the degree of deviation of the line shape from a Gaussian. In Section 2 we review our simulation suite and the method from Lovell et al. (2019), then present our results in Section 3 and draw conclusions in Section 4.

2. Simulations and Methods

We use the 30 hydrodynamical simulations of cluster zooms included in the C-EAGLE project, which are described in full in Bahé et al. (2017) and Barnes et al. (2017). Briefly, the galaxy formation model is the AGNdT9 version of the EAGLE model (Schaye et al. 2015), which features cooling, star formation, supernova feedback, and black hole growth and feedback; the AGNdT9 model is optimized over the standard EAGLE reference model to improve the gas-to-total-mass fractions and X-ray luminosity–temperature relations in massive clusters. The dark matter particle mass is $9.7 \times 10^6 M_\odot$, the softening length is 0.7 kpc at $z = 0$, and the cosmological parameters were chosen to be consistent with the Planck Collaboration et al. (2014) results: Hubble parameter, $h = H_0 / (100 \text{ km s}^{-1}) = 0.6777$; dark energy density, $\Omega_\Lambda = 0.693$; matter density $\Omega_M = 0.307$; and baryon energy density $\Omega_b = 0.04825$.

The method for determining the dark matter decay flux is the same as that first presented in Lovell et al. (2015) and expanded in Lovell et al. (2019). To summarize, we place an observer at a distance of 69.5 Mpc—i.e., the distance to Perseus—from the center of the most massive galaxy in each simulated cluster, draw a cone determined by the field of view (FoV) of the *XRISM* telescope (which we treat as a circle of radius $1'4$) and the observer–cluster axis (radius 28 kpc at the cluster center); we have also performed these analyses with the *ATHENA/XIFU* FoV ($2'5$; 50 kpc aperture radius at the Perseus distance), which is very similar in its FoV and spectral resolution to the proposed *Lynx/LXM* instrument. Having chosen an FoV, we identify the dark matter particles located within the cone delineated by that FoV. We treat each dark matter particle as a point source of decay photons emitted isotropically at a constant rate.

The decay flux is then the total flux measured from dark matter particles within the FoV; we do not add any contribution from intervening dark matter unassociated with the cluster. The shape of the line—and thus its dispersion and full width at half maximum (FWHM)—are calculated by binning the flux from each particle in line-of-sight (l.o.s., i.e., 1D) velocity. We repeat this process for 500 observer locations distributed at random on a sphere of radius 69.5 Mpc. For each halo we select our galaxy and dark matter particle locations from the $z = 0$ simulation snapshot, which is a good approximation for the Perseus cluster ($z = 0.0167$). The one difference from the mock Perseus observations reported in Lovell et al. (2019) is that we select particles up to 10 Mpc from the cluster center for analysis, as opposed to 2 Mpc in that previous study, to ensure we include the contribution to the line profile of any high velocity infalling dark matter.

We calculate the 1D cluster galaxy velocity dispersion in a way that mirrors the procedure of Tamura et al. (2014), who used CfA and CMASS redshifts for 100 galaxies within $30'$ of the center of Perseus. Using the same 500 observer positions calculated for the X-ray flux mock observations, we draw a cone defined by the cluster center/observer axis and an opening angle of $30'$ (radius 600 kpc at the halo center, which is a third of the virial radius). We select the first 100 galaxies in the halo/subhalo catalog, ranked by halo mass, of which the center-of-potential is located within this cone and compute their 1D velocity dispersion along the line of sight associated with that observer. For each of the 500 observers we therefore measure two velocity dispersions (σ_{1D}): one for the dark matter particles, $\sigma_{1D,DM}$, and one for the member galaxies, $\sigma_{1D,gals}$.

We repeat the $\sigma_{1D,gals}$ procedure for the observed Perseus galaxies of the Tamura et al. (2014) sample, and obtain an observed velocity dispersion of 1210 km s^{-1} if the bright, CMASS galaxies are used and 1330 km s^{-1} if the CfA galaxy sample is used, both of which are in broad agreement with the older measurement of Kent & Sargent (1983). For the purposes of this paper we take the approximate limit on the value of the observed 1D velocity dispersion of Perseus galaxies to be $[1200, 1400] \text{ km s}^{-1}$. We will compare these values specifically to those halos that have the same measured virial mass, M_{200} , as Perseus, where M_{200} is defined as the mass within the radius that encloses an overdensity 200 times the critical density of the universe. We adopt the Perseus M_{200} to be $6.65^{+0.43}_{-0.46} \times 10^{14} M_{\odot}$ (Simionescu et al. 2011), and the halos that match this M_{200} range are halos 18 ($6.94 \times 10^{14} M_{\odot}$) and 19 ($6.84 \times 10^{14} M_{\odot}$). Finally, we repeat parts of this analysis

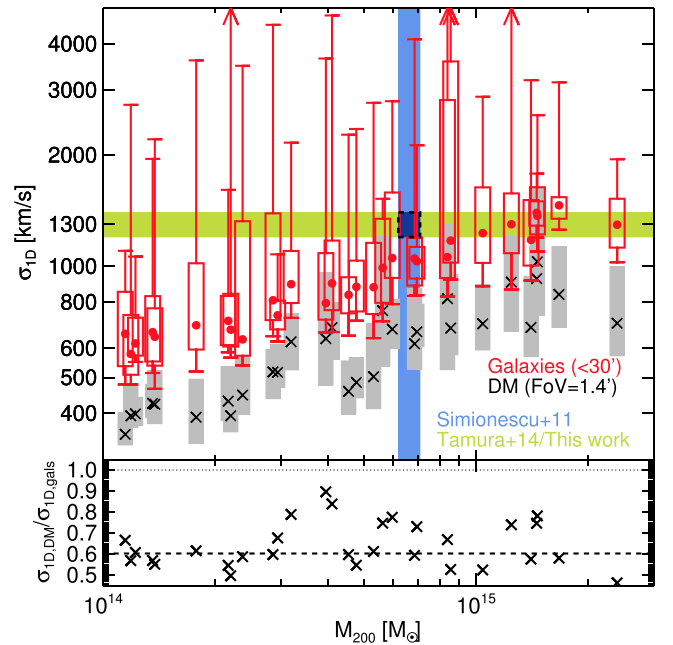


Figure 1. Top panel: C-EAGLE cluster dark matter and galaxy velocity dispersions as a function of halo mass. The median values of $\sigma_{1D,DM}$ over 500 sightlines are plotted as black crosses, and the region encompassing 95% of the data for each halo as a gray rectangle. Similarly, the median $\sigma_{1D,gals}$ are shown as red circles, and the error bars the 95% region; in cases where the upper 95% limit is above 5000 km s^{-1} , that upper limit is truncated and represented by an arrow. The Perseus value of $\sigma_{1D,gals}$ that we measure using the Tamura et al. (2014) data is plotted as a green band. The blue band is the measured range of M_{200} for Perseus ($6.19\text{--}7.02 \times 10^{14} M_{\odot}$). Bottom panel: the ratios of the median $\sigma_{1D,DM}$ and $\sigma_{1D,gals}$. The median ratio of $\sigma_{1D,DM}$ relative to $\sigma_{1D,gals}$ is shown as a dashed line.

for three further clusters—Ophiuchus, Virgo, and Centaurus—and present those results in the supplementary material.

3. Results

We begin the presentation of our results by showing the differences between $\sigma_{1D,DM}$ and $\sigma_{1D,gals}$ for clusters across the mass range $1 \times 10^{14}\text{--}2 \times 10^{15} M_{\odot}$, and then how those with the Perseus mass compare to the observationally measured Perseus $\sigma_{1D,gals}$. In Figure 1 we plot $\sigma_{1D,DM}$ and $\sigma_{1D,gals}$ for all 30 C-EAGLE halos as a function of M_{200} .

The difference between the values of the two sets of velocity dispersion is significant. At all halo masses, the median $\sigma_{1D,gals}$ is about 70% higher than $\sigma_{1D,DM}$.⁷ Clearly, taking the Kent & Sargent (1983) $\sigma_{1D,gals} = 1300 \text{ km s}^{-1}$ —the value for $\sigma_{1D,gals}$ adopted by Aharonian et al. (2017)—as a proxy for the velocity dispersion of a dark matter decay line is a large overestimate. Our calculation also shows that the $\sigma_{1D,gals}$ in the C-EAGLE simulations are in good agreement with the value inferred from the CMASS and CfA data. This high value is similar to that found for the same data sets by Armitage et al. (2019), who also showed that cluster galaxy orbits are preferentially radial rather than tangential; a similar result for a different data set was shown by Elahi et al. (2018).

We now check whether there is any correlation between $\sigma_{1D,gals}$ and $\sigma_{1D,DM}$ for each halo, by calculating the Spearman’s

⁷ The scatter is also much higher for $\sigma_{1D,gals}$ than for $\sigma_{1D,DM}$: this is due to the sampling error difference between taking 100 galaxies versus millions of dark matter particles.

rank correlation coefficient across the 500 sightlines for each of the 30 halos. We then test the significance of these coefficients by comparing the results to 10,000 randomly drawn sets of 500 ranked-pairs, and also by applying a Fisher transformation/ z -score test. Under both tests, only 4 of the 30 halos showed Spearman coefficients consistent with the null hypothesis that there is no correlation between $\sigma_{\text{ID,gals}}$ and $\sigma_{\text{ID,DM}}$ at three standard deviations. Twenty-five showed a significant preference for a positive correlation and the last one showed a strong preference for an anticorrelation.

We focus the rest of our analysis on those sightlines that best describe Perseus as per our constraints. These are the sightlines that run through Perseus-mass halos and have the measured Perseus galaxy velocity dispersion, i.e., those that are enclosed by dashed lines at the intersection of the bands in Figure 1. We thus choose those sightlines that belong to the two halos that are within the measured mass range for Perseus—halos 18 and 19—and have $\sigma_{\text{ID,gals}}$ in the range [1200, 1400] km s⁻¹, of which there are only 37 since the measured Perseus $\sigma_{\text{ID,gals}}$ is significantly above the median simulated $\sigma_{\text{ID,gals}}$ at this halo mass range. We dub these “Perseus-analog” sightlines; however, the values of the Spearman correlation coefficient in $\sigma_{\text{ID,gals}}-\sigma_{\text{ID,DM}}$ for these two halos are only 0.37 and 0.26, so our results are not strongly influenced by this choice.

The total flux of the line is anticipated from the mass and, to a lesser extent, the concentration of the Perseus halo (as computed, for example, in Lovell et al. 2019), while the line width can be estimated from the virial theorem alongside assumptions about the anisotropy of dark matter particle orbits. The line shape is typically assumed to be a Gaussian. We test the degree of deviation from the Gaussian in the following manner. For each of our subsamples of Perseus-analog sightlines we compute the unique Gaussian that has the same total flux and FWHM as each sightline and then calculate the ratio of the difference between the simulation sightline and the Gaussian approximation, i.e.,

$$\text{ratio}(v) = \frac{f_{\text{sim}}(v) - f_{\text{gauss}}(v)}{f_{\text{gauss}}(v)}, \quad (1)$$

where $f_{\text{sim}}(v)$ and $f_{\text{Gauss}}(v)$ are the line profiles measured from the simulation and using the Gaussian approximation respectively. We also reflect each Perseus-analog curve about velocity $v = 0$ if necessary to ensure that there is more flux at positive velocities than at negative, thus maximizing the visibility of any line asymmetry present. In Figure 2, we plot each line difference ratio as a thin line. We also plot three sets of median relations defined by the value of the ratio at the velocity, $v = 0$ km s⁻¹: the $\sim 15\%$ that have the highest ratio value at $v = 0$ km s⁻¹ and also the $\sim 15\%$ lowest.

Within 1000 km s⁻¹ either side of the line centroid, the deviation from the Gaussian line profile is typically less than 20%. The median differences of the subsample are deficits of 10% at the centroid, 5% at $v = +700$ km s⁻¹ and 20% at $v = -700$ km s⁻¹, suggesting that any asymmetry of the line could be detectable with the *XRISM* energy resolution. These values are suppressed by a further 5%–10% for the low-peak subsample, and correspond to simulated curves that have broader tails than the Gaussian as show by the sharply increasing ratio values for velocity $|v| > 1000$ km s⁻¹. This excess of flux at large velocities is also apparent in the high-peak subsample, where the peak value is 10% higher than the

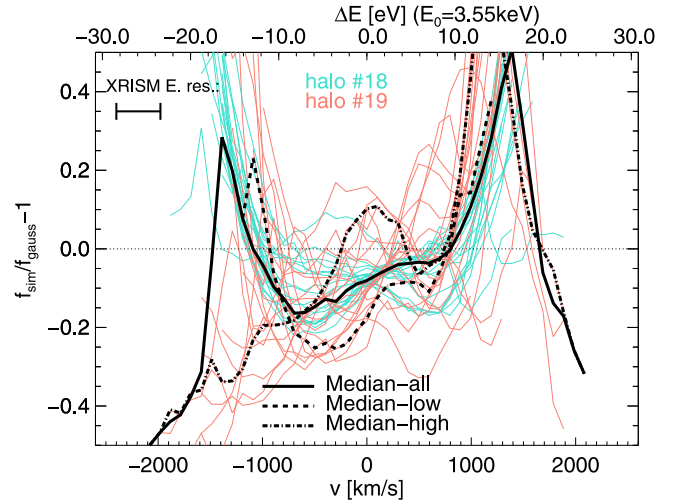


Figure 2. Ratio of the difference between each Perseus-analog velocity profiles relative to a Gaussian line with the same FWHM and total flux amplitude. Individual sightlines are plotted as thin lines and are colored according to host halo (turquoise and pink). Median relations are plotted as thick black lines: a solid line for the whole sample, dashed for the high-ratio subsample and dotted-dashed for the low ratio subsample. We plot the velocities on the lower x -axis and energies on the upper x -axis (both rest frames), where the energy scale assumes an emission energy $E_0 = 3.55$ keV. The velocity/energy resolution of the *XRISM* instrument is shown in the top left corner.

Gaussian but otherwise follows the pattern of a deficit at $|v| = 700$ km s⁻¹ and an enhancement at larger velocities. We note that there is an apparent difference between the two halos, with the Gaussian providing a better match to the halo 18 curves than to those of halo 19; this is likely because halo 19 is less relaxed than halo 18 (Barnes et al. 2017). Finally, we have repeated this exercise with a series of sightlines offset from the halo center by $1'$, as used for some of the *Hitomi* observations, and find no significant differences to our on-center results. We conclude that a Gaussian is an appropriate approximation to the proposed Perseus dark matter decay line at the 20% level, and otherwise the biggest difference is in the presence of broader tails in the distribution. For the remainder of this Letter, we use the $\sigma_{\text{ID,DM}}$ measured directly from the simulations, and not that from a Gaussian fit.

We now present some predictions for the properties of the line to be probed by the *XRISM* satellite: $\sigma_{\text{ID,DM}}$ and flux, F . We present our results as a series of contours in $\sigma_{\text{ID,DM}}$ and F for mock observations made with the *XRISM* FoV (using a circular aperture of radius $1'.4$), assuming a dark matter particle mass of 7.1 keV and a particle lifetime of 1×10^{28} s.⁸ We draw one set of contours for each of the halos that we consider, using all 500 on-center sightlines, and plot the 37 Perseus-analog on-center sightlines as circles. We also include the Perseus-analog sightlines from our off-center ($1'$) observations, which is the off-center angle in some of the *Hitomi* observations, as squares. Each off-center mock observation was performed from the same observer location as one of the on-center observations, and we indicate which off-center–on-center pairs share a common observer position using solid lines. We present these results in Figure 3.

Both halos’ $F-\sigma_{\text{ID,DM}}$ distributions are highly asymmetric, with a preference for $F \sim 5 \times 10^{-8}$ counts s⁻¹ cm⁻² and a long tail to fluxes almost twice as large. There is also a slight

⁸ Note that the flux is inversely proportional to both the particle mass and the lifetime but the velocity dispersion is independent of these parameters.

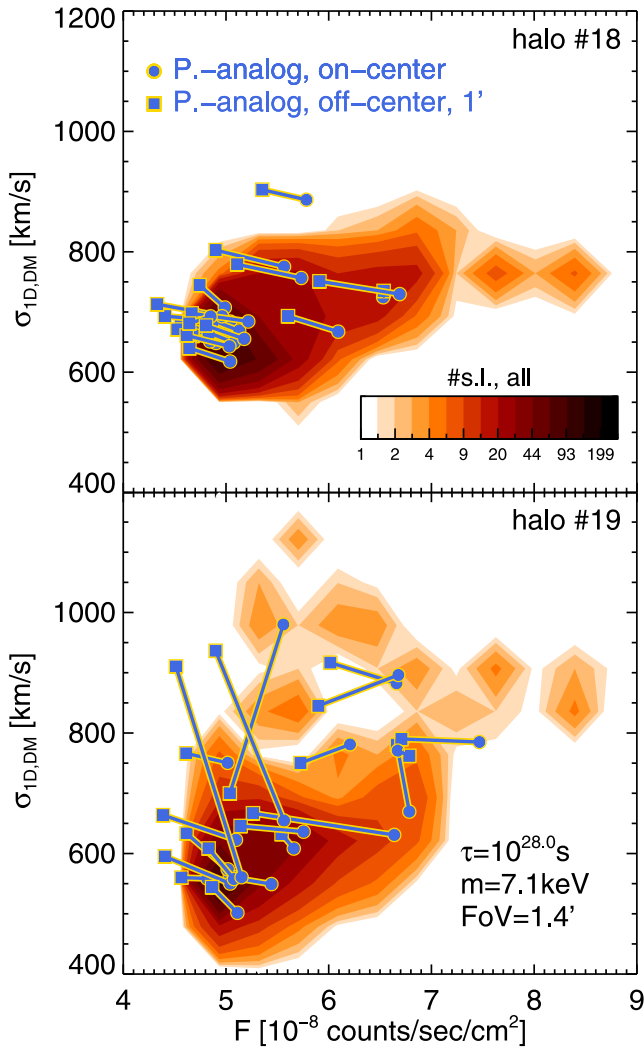


Figure 3. Heat map plots in $\sigma_{1D,DM}$ and in flux, F for all 500 halo 18 (top panel) and halo 19 (bottom panel) on-center sightlines (s.l.). The color bar indicates the number of s.l. in each contour cell, and we use the same color bar for both panels. The Perseus-analog sightlines are shown as blue circles. 1' off-center counterparts to the Perseus-analog sightlines are shown as blue squares, and are linked to their corresponding on-center observations with solid lines.

preference for a correlation between F and $\sigma_{1D,DM}$. The spread in $\sigma_{1D,DM}$ values is twice as large for the less relaxed halo 19 as for the more relaxed halo 18; for both halos $\sigma_{1D,DM}$ is significantly more than the 180 km s $^{-1}$ dispersion derived for the hot cluster gas in Aharonian et al. (2017). Differences in halo formation history/asymmetry are important for the properties of the signal. Evidence for this difference between relaxed and unrelaxed halos comes in the relationship between the on- and off-center observations of Perseus-analog sightlines. The halo 18 subsample shows a remarkably regular preference for the off-center sightlines to have lower flux and slightly higher $\sigma_{1D,DM}$ than their on-center counterparts, with a median 3.9×10^{-9} counts s $^{-1}$ cm $^{-2}$ decrement in flux and 18 km s $^{-1}$ enhancement in $\sigma_{1D,DM}$. By contrast, the halo 19 Perseus-analog sightlines show a much greater range of behaviors, from increases in $\sigma_{1D,DM}$ of 350 km s $^{-1}$ from on-center to off-center, to the same change in the opposite direction. An in-depth prediction would require constrained simulations of Perseus-analog halos that are beyond the scope of this Letter. Finally, we have repeated this exercise using the

ATHENA/XIFU FoV, which we approximate as a circle of radius $2\sqrt{5}$. We obtain results similar to those for *XRISM*, with the following exceptions: the range of flux is $[1.1-2.1] \times 10^{-7}$ counts s $^{-1}$ cm $^{-2}$; the high-flux tail for halo 18 shows an increased $\sigma_{1D,DM} \sim 870$ km s $^{-1}$ and is therefore the same as that of halo 19; and the differences between the on- and off-center observations shrink in relative terms, both for F and for $\sigma_{1D,DM}$.

4. Conclusions

If the dark matter is a particle that decays, the Perseus galaxy cluster is an excellent target for which to collect data suitable for indirect detection. The interpretation of the observations requires an estimate of the decay line amplitude, width, and shape. In this Letter, using the C-EAGLE cosmological hydrodynamical simulations of massive clusters, we have calculated these three line properties and explore how they correlate with the Perseus halo properties.

We showed that the 1D velocity dispersion of the dark matter—as measured within the *Hitomi/XRISM* FoV—is typically 40% smaller than the 1D velocity dispersion of the cluster member galaxies when evaluated using members within 30' of the cluster center (Figure 1). We showed that there is a correlation between the two velocity dispersions, but it is very weak and not present for all 30 simulated halos. We confirmed that the line profile is well described by a Gaussian within 1000 km s $^{-1}$ of the line center, although the presence of line asymmetry is common (Figure 2). We also presented estimates of the distributions of fluxes and dark matter velocity dispersions for different lines of sight, and found that both could vary by as much as a factor of two. This is particularly true if the halo is unrelaxed, in which case there can be dramatic differences between the line profiles on- and off-center (Figure 3). These differences are much smaller when the larger *ATHENA/XIFU* FoV is used; otherwise, the results from that instrument are similar to those for the *XRISM* FoV.

In summary, we have shown that the velocity dispersion of the proposed dark matter decay line in Perseus is much smaller than the velocity dispersion of cluster galaxies. We predict that, if the reported 3.55 keV line does indeed originate from dark matter decay, the upcoming observations of Perseus by the *XRISM* mission—assuming an exposure time of 1 Ms (Bulbul et al. 2014)—will detect a line with the following properties: a total flux of $[4, 9] \times 10^{-8}$ counts s $^{-1}$ cm $^{-2}$, a velocity dispersion of $[600, 800]$ km s $^{-1}$ —although exceptionally as large as 1200 km s $^{-1}$ —and a shape that is within 20% of Gaussian.

M.R.L. is supported by a COFUND/Durham Junior Research Fellowship under EU grant 609412 and also by a Grant of Excellence from the Icelandic Research Fund (grant No. 173929051). D.I. acknowledges support from the grant for young scientists research laboratories of the National Academy of Sciences of Ukraine. C.S.F. acknowledges a European Research Council Advanced Investigator grant DMIDAS (GA 786910) and support for the STFC Consolidated Grant for Astronomy at Durham. This work used the DiRAC@Durham facility managed by the Institute for Computational Cosmology on behalf of the STFC DiRAC HPC Facility (www.dirac.ac.uk). The equipment was funded by BEIS capital funding via STFC capital grants ST/K00042X/1, ST/P002293/1, ST/R002371/1, and ST/S002502/1, Durham University and STFC operations grant ST/R000832/1. DiRAC is part of the

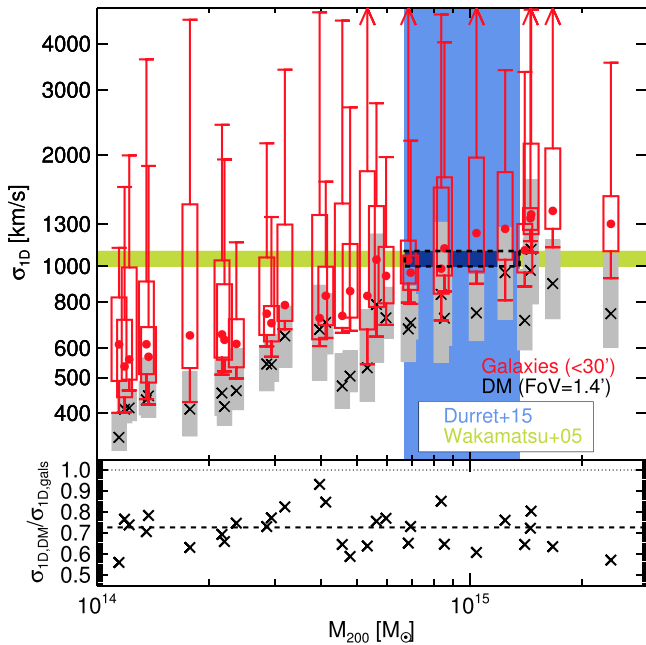


Figure 4. Repetition of Figure 1 for halos placed at the Ophiuchus redshift, where the observations are given by the measured Ophiuchus values.

National e-Infrastructure. W.A.H. is supported by an Individual Fellowship of the Marie Skłodowska-Curie Actions and therefore acknowledges that this project has received funding from the European Union’s Horizon 2020 research and innovation program under the Marie Skłodowska-Curie grant agreement No. 748525.

Appendix A Supplementary Information

In this supplementary information we replicate Figures 1 and 3 of our Perseus analysis for three other clusters: Virgo, Centaurus, and Ophiuchus. We choose these three clusters because they were used as part of some prominent subsamples of the Bulbul et al. (2014) analysis. All of the methodology applied is the same as Perseus, including a 30’ opening angle/100 member galaxy sample for the cluster galaxy velocity dispersion. Another cluster of interest is Coma; however, the measured mass and redshift for Coma are very similar to that of Perseus, so the results are likely to be very similar to our Perseus results and therefore we do not repeat the analysis for Coma.

Appendix B Ophiuchus

Ophiuchus is one the closest large ($M > 10^{15} M_{\odot}$) galaxy clusters to the Milky Way. For our purposes, Ophiuchus is a cluster with a redshift $z = 0.028$ (~ 120 Mpc, or 75% further away than Perseus), a mass $M_{200} = 11^{+4.3}_{-2.6} \times 10^{14} M_{\odot}$ (Durret et al. 2015), and a velocity dispersion of $\sigma_{\text{ID,gals}} = [1000, 1100] \text{ km s}^{-1}$; the velocity dispersion was calculated using galaxies within 30’ of the cluster center, just like Perseus (Wakamatsu et al. 2005). We present the results for our clusters located at $z = 0.028$ in Figure 4; we adopt the *XRISM* FoV.

Unlike Perseus, the measured Ophiuchus galaxy velocity dispersion is well within the 68% region for the simulated

$\sigma_{\text{ID,gals}}$ in the allowed mass range. The difference between the galaxy and dark matter velocity dispersions is smaller than was the case for Perseus, with an average ratio of 30%: we expect this is because the cluster is 75% further away than Perseus and so the 30’ FoV encompasses more galaxies with low (l.o.s.) relative velocities in the plane of the sky. There are six halos that fall within the measured mass range for Ophiuchus; we plot the $\sigma_{\text{ID,DM}}-F$ contours for these six halos in Figure 5.

The six halos consistently show a preference for $F \sim 4 \times 10^{-8} \text{ counts s}^{-1} \text{ cm}^{-2}$, with a long tail that extends to $6 \times 10^{-8} \text{ counts s}^{-1} \text{ cm}^{-2}$. The dark matter velocity dispersion is much more variable: although all six halos present $\sigma_{\text{ID,DM}}$ in the range $[600, 1000] \text{ km s}^{-1}$, some halos show a positive correlation between the two quantities (halos 18 and 19), whereas 22 presents a negative correlation. Halos 23 and 24 also present a small subset of $\sigma_{\text{ID,DM}} > 1200 \text{ km s}^{-1}$. In general the $\sigma_{\text{ID,gals}}$ -selected sightlines show similar behavior to Perseus, with off-center fluxes suppressed at the tens of percent level compared to their on-center counterparts, with the off-center $\sigma_{\text{ID,DM}}$ values typically enhanced at the $<10\%$ level. With the possible exception of low flux-high dispersion sightlines, the $\sigma_{\text{ID,gals}}$ subsample is not consistently biased relative to the full 500 sightlines.

Appendix C Virgo

The Virgo cluster is the closest cluster to the MW, and thus an important candidate for dark matter indirect detection. It is located at a redshift 0.0036 (~ 16 Mpc, 22% of the distance to Perseus), the galaxy velocity dispersion is $632^{+41}_{-29} \text{ km s}^{-1}$ (~ 500 member galaxies; Fadda et al. 1996), and the halo mass $M_{200} = (1.05 \pm 0.02) \times 10^{14} M_{\odot}$ (Simionescu et al. 2017). Our comparison between C-EAGLE cluster velocity dispersion at the Virgo distance and the Virgo data is shown in Figure 6.

The difference between the galaxy and dark matter velocity dispersions is stronger than was the case for Perseus, with the galaxy velocity dispersion on average a factor of 2 larger than the dark matter velocity dispersion. Virgo is therefore in some ways the opposite of Ophiuchus: it is much closer than Perseus, so our 30’ subtends a smaller part of the halo radius and thus only selects the high l.o.s. velocity galaxies, given that the galaxy orbits are preferentially radial. The measured Virgo velocity dispersion is located squarely within the 68% region of our three lowest mass clusters. None of the clusters has a mass within the 1σ error bar derived by Simionescu et al. (2017); we proceed with taking just the lowest mass halo in the sample, halo 1, to be a Virgo analog; for a discussion of halo-to-halo scatter we refer the reader back to the section on Ophiuchus.

The most likely observed dark matter decay flux for Virgo, as modeled by halo 1 in Figure 7, is $\sim 0.9 \times 10^{-7} \text{ counts s}^{-1} \text{ cm}^{-2}$, and the high-flux tail extends to $\sim 1.4 \times 10^{-7} \text{ counts s}^{-1} \text{ cm}^{-2}$. The velocity dispersion sits in the range of $[420, 540] \text{ km s}^{-1}$. By comparing to the Ophiuchus results in Figure 5, we expect that similar halos of the same mass may present similar ranges in flux and velocity dispersion but potentially with a population of high flux—high velocity dispersion sightlines that are not present for halo 1. The scatter between the velocity dispersions of the $\sigma_{\text{ID,gals}}$ selected sample, relative to the change in flux, is bigger than for Ophiuchus, which likely reflects the extra variation between sightlines when using an aperture that is small relative to the angular size of the cluster.

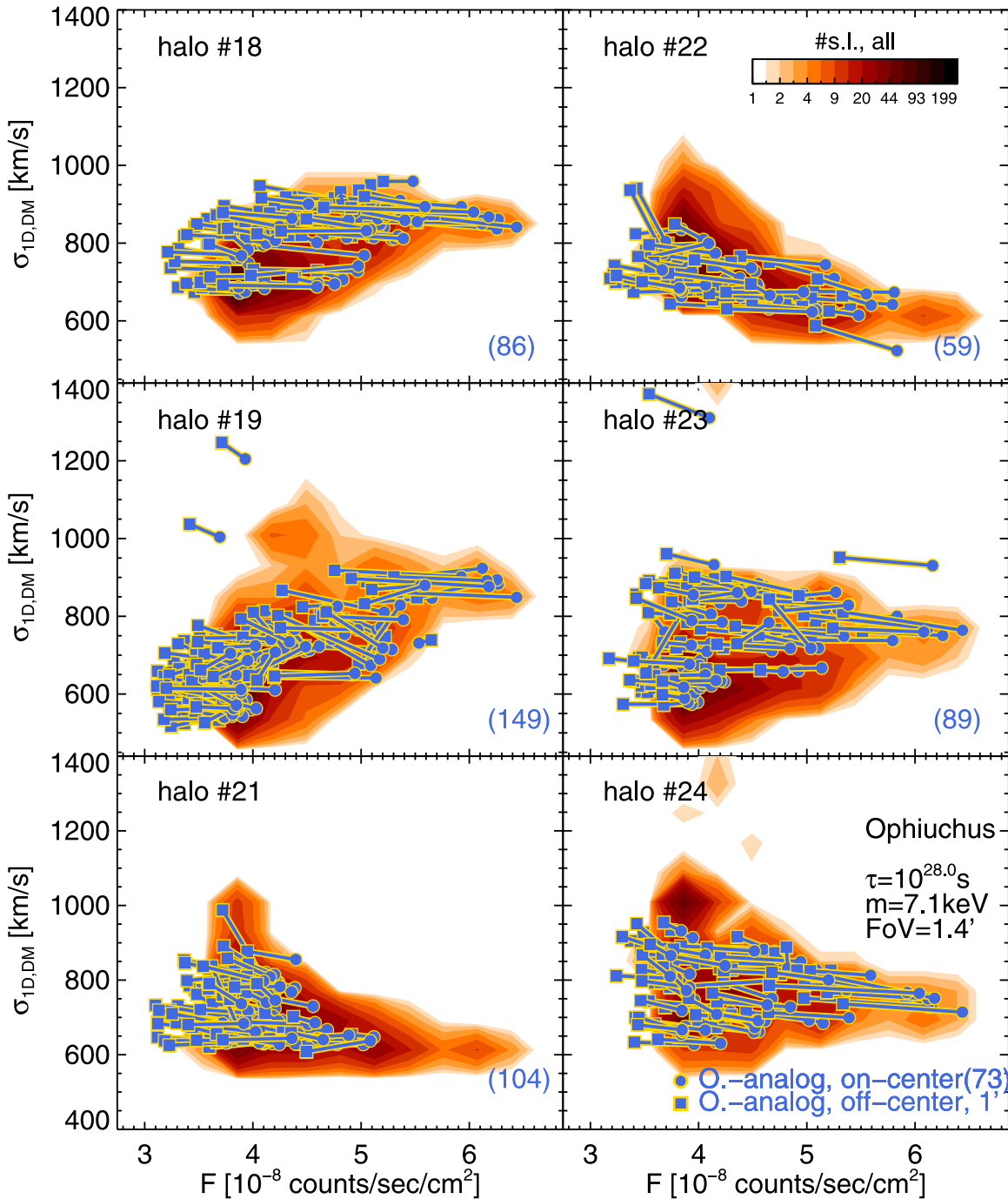


Figure 5. Repetition of Figure 3 for Ophiuchus, using the six halos that match the Ophiuchus M_{200} ; each halo is presented in a separate panel. The number of $\sigma_{1D,\text{gal}}$ -selected sightlines in each panel is shown in brackets.

Appendix D Centaurus

Finally, we present results for the Centaurus cluster, which is located at a redshift $z = 0.0109$ (~ 48 Mpc, 68% of the distance to Perseus). It has a measured mass $M_{200} = 1.6_{-0.2}^{+0.3} \times 10^{14} M_{\odot}$ (Walker et al. 2013). The velocity dispersion measurement is complicated by the apparent presence of two peaks in the velocity distribution (Fadda et al. 1996); we adopt the velocity dispersion that Fadda et al. (1996) derived for this cluster $79_{-62}^{+60} \text{ km s}^{-1}$ and comment below on the possible impact of substructure. The comparison between the galaxy and dark matter velocity dispersions is presented in Figure 8.

The dark matter velocity dispersions are suppressed by 40% relative to the galaxy velocity dispersions, which is similar to Perseus. The measured $\sigma_{1D,\text{gal}}$ is in agreement with the simulation predictions, although at the higher end of the allowed region, which is consistent with the presence of a small subcluster along the line of sight. Only one of our halos—halo 4—has a mass within the measured range for Centaurus; we adopt this one halo as our Centaurus analog, and again refer back to the Ophiuchus results for a discussion of halo-to-halo scatter.

The distribution of halo 4 sightlines, as shown in Figure 9, prefers a flux of $0.6 \times 10^{-7} \text{ counts s}^{-1} \text{ cm}^{-2}$ with a tail

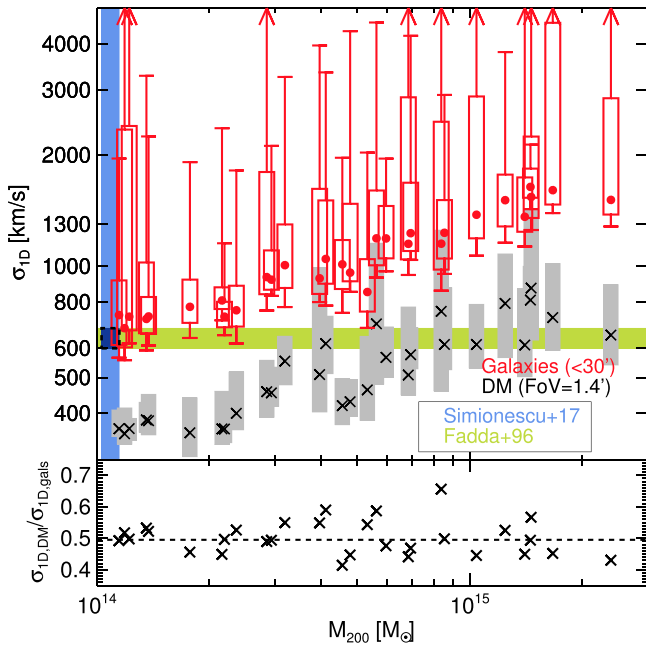


Figure 6. Repetition of Figure 1’s analysis for the clusters at the Virgo redshift. The Virgo value of $\sigma_{\text{ID,gals}}$ measured by Fadda et al. (1996) is shown as a green band, and the blue band is the allowed range of M_{200} for Virgo: $M_{200} = (1.03\text{--}1.07) \times 10^{14} M_{\odot}$ (Simionescu et al. 2017).

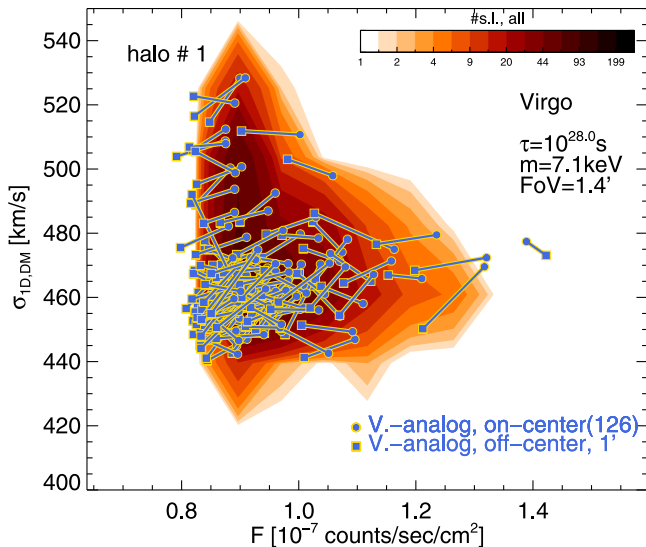


Figure 7. Repetition of Figure 3 for Virgo, using halo 1 from our sample placed at the Virgo redshift.

maximum of $0.9 \times 10^{-7} \text{ counts s}^{-1} \text{ cm}^{-2}$. The range of allowed velocity dispersions is $[380, 500] \text{ km s}^{-1}$, with a small minority of sightlines preferring a much higher $\sigma_{\text{ID,DM}} \sim 650 \text{ km s}^{-1}$. The velocity dispersion is largely independent of flux; we anticipate from Figure 5 that other halos would show a weak trend, however. Finally, we note that the Centaurus $\sigma_{\text{ID,DM}}$ -selected sightlines show a clear preference for off-center fluxes to be suppressed at tens of percent and $\sigma_{\text{ID,DM}}$ to be enhanced at less than 10%.

ORCID iDs

Mark R. Lovell <https://orcid.org/0000-0001-5609-514X>
Sownak Bose <https://orcid.org/0000-0002-0974-5266>

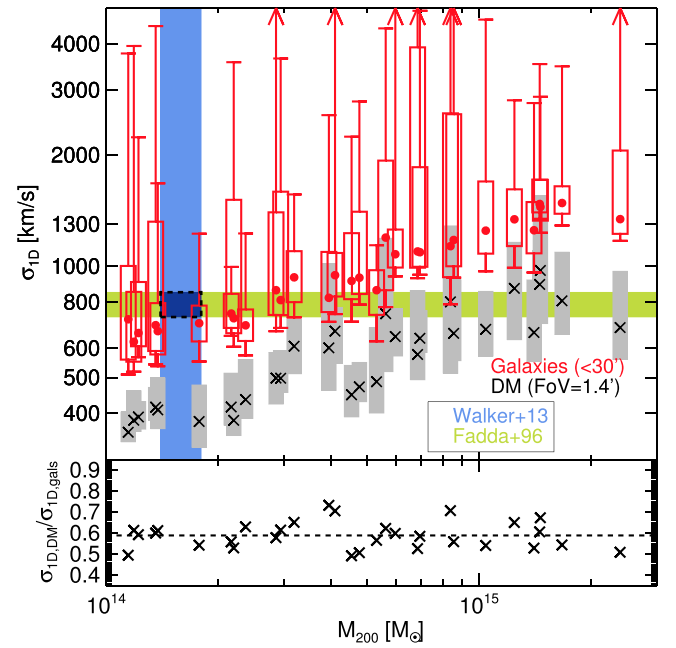


Figure 8. Repetition of the Figure 1 analysis for the C-EAGLE clusters when placed at the redshift of Centaurus ($z = 0.0109$).

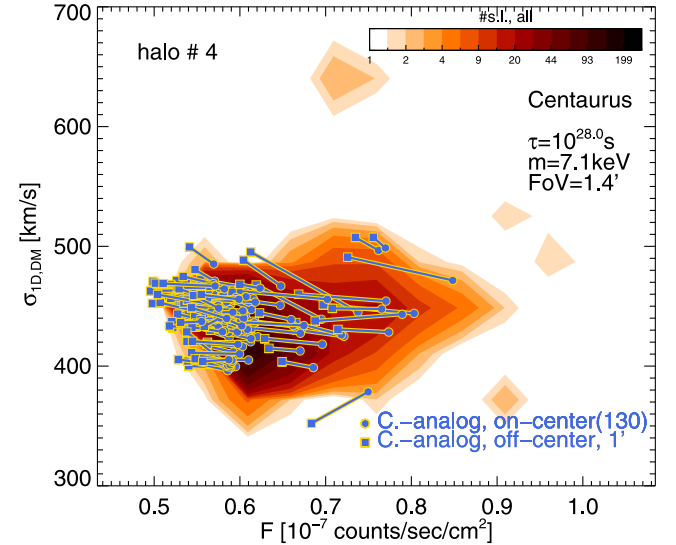


Figure 9. Repetition of Figure 3 for halo 4 when placed at the Centaurus redshift.

References

- Aharonian, F. A., Akamatsu, H., Akimoto, F., et al. 2017, *ApJL*, **837**, L15
Armitage, T. J., Barnes, D. J., Kay, S. T., et al. 2018, *MNRAS*, **474**, 3746
Armitage, T. J., Kay, S. T., Barnes, D. J., Bahé, Y. M., & Dalla Vecchia, C. 2019, *MNRAS*, **482**, 3308
Bahé, Y. M., Barnes, D. J., Dalla Vecchia, C., et al. 2017, *MNRAS*, **470**, 4186
Barnes, D. J., Kay, S. T., Bahé, Y. M., et al. 2017, *MNRAS*, **471**, 1088
Boyarisky, A., Iakubovskiy, D., Ruchayskiy, O., & Savchenko, D. 2018, arXiv:1812.10488
Boyarisky, A., Ruchayskiy, O., Iakubovskiy, D., & Franse, J. 2014, *PhRvL*, **113**, 251301
Bulbul, E., Markevitch, M., Foster, A., et al. 2014, *ApJ*, **789**, 13
Cappelluti, N., Bulbul, E., Foster, A., et al. 2018, *ApJ*, **854**, 179
Durret, F., Wakamatsu, K., Nagayama, T., Adami, C., & Biviano, A. 2015, *A&A*, **583**, A124
Elahi, P. J., Power, C., Lagos, C. d. P., Poulton, R., & Robotham, A. S. G. 2018, *MNRAS*, **477**, 616

- Fadda, D., Girardi, M., Giuricin, G., Mardirossian, F., & Mezzetti, M. 1996, [ApJ](#), **473**, 670
- Kent, S. M., & Sargent, W. L. W. 1983, [AJ](#), **88**, 697
- Lovell, M. R., Barnes, D., Bahé, Y., et al. 2019, [MNRAS](#), **485**, 4071
- Lovell, M. R., Bertone, G., Boyarsky, A., Jenkins, A., & Ruchayskiy, O. 2015, [MNRAS](#), **451**, 1573
- Planck Collaboration, Ade, P. A. R., Aghanim, N., et al. 2014, [A&A](#), **571**, A16
- Schaye, J., Crain, R. A., Bower, R. G., et al. 2015, [MNRAS](#), **446**, 521
- Simionescu, A., Allen, S. W., Mantz, A., et al. 2011, [Sci](#), **331**, 1576
- Simionescu, A., Werner, N., Mantz, A., Allen, S. W., & Urban, O. 2017, [MNRAS](#), **469**, 1476
- Tamura, T., Fabian, A. C., Gandhi, P., et al. 2018, [PASJ](#), **42**, psz023
- Tamura, T., Yamasaki, N. Y., Iizuka, R., et al. 2014, [ApJ](#), **782**, 38
- Wakamatsu, K., Malkan, M. A., Nishida, M. T., et al. 2005, in ASP Conf. Ser. 329, Nearby Large-Scale Structures and the Zone of Avoidance, ed. A. P. Fairall & P. A. Woudt (San Francisco, CA: ASP), 189
- Walker, S. A., Fabian, A. C., Sanders, J. S., Simionescu, A., & Tawara, Y. 2013, [MNRAS](#), **432**, 554